PHULAD SHEAR ZONE, RAJASTHAN, NW INDIA: THE PROPOSED MID-NEOPROTEROZOIC SUTURE FOR THE GREATER INDIA LANDMASS

Sadhana M Chatterjee*, Manideepa Roy Choudhury, Subhrajyoti Das and Alip Roy
Department of Geological Sciences, Jadavpur University, 188, Raja S. C. Mallick Road, Jadavpur, Kolkata, 700032, India, * E-mail: smcjugeo@gmail.com

GSA Annual Meeting in Seattle, Washington, USA - 2017, October 22 to 25, 2017

1. Introduction:

The position and participation of the Greater India landmass within the Rodinia supercontinent has been widely debated. Profound similarities between the Grenvillian age domain in the Eastern Ghats Granulite Belt, India and the Rayner Complex, Antarctica has prompted researchers to suggest that India and Australo-Antarctic Block formed a coherently evolving landmass within Rodinia during the Grenville. Palaeomagnetic studies from Malani Igneous Suite (MIS) in the Marwar Craton of northwestern India, on the other hand, place India far removed from the Rodinia landmass.

In northwestern India the Phulad Shear Zone (PSZ) demarcates the boundary between Grenvillian-age South Delhi Fold Belt (SDFB) to the east and Neoproterozoic granitoids of the Marwar Craton to the west (Figure 1). Review of available age data in the SDFB and in the adjoining Marwar Craton shows two distinct age populations. The older 1000–900 Ma ages in the SDFB are identical to those recorded in the banded gneissic complex farther east. The younger set of Neoproterozoic ages (800–750 Ma) are prevalent along the western parts of the SDFB and in large parts of the Marwar Craton but are lacking eastward within the Aravalli Delhi Fold Belt (ADFB). Although 800–750 Ma ages are commonly recorded in metamorphic rocks and in granitoids in northwestern India, their tectonic significance is poorly understood. In this work, we study Neoproterozoic tectonism based on detailed analyses of deformation structures, metamorphic pressure-temperature (P-T) path reconstruction, and monazite chemical age determinations in and around Phulad, the type section for the crustal-scale PSZ.

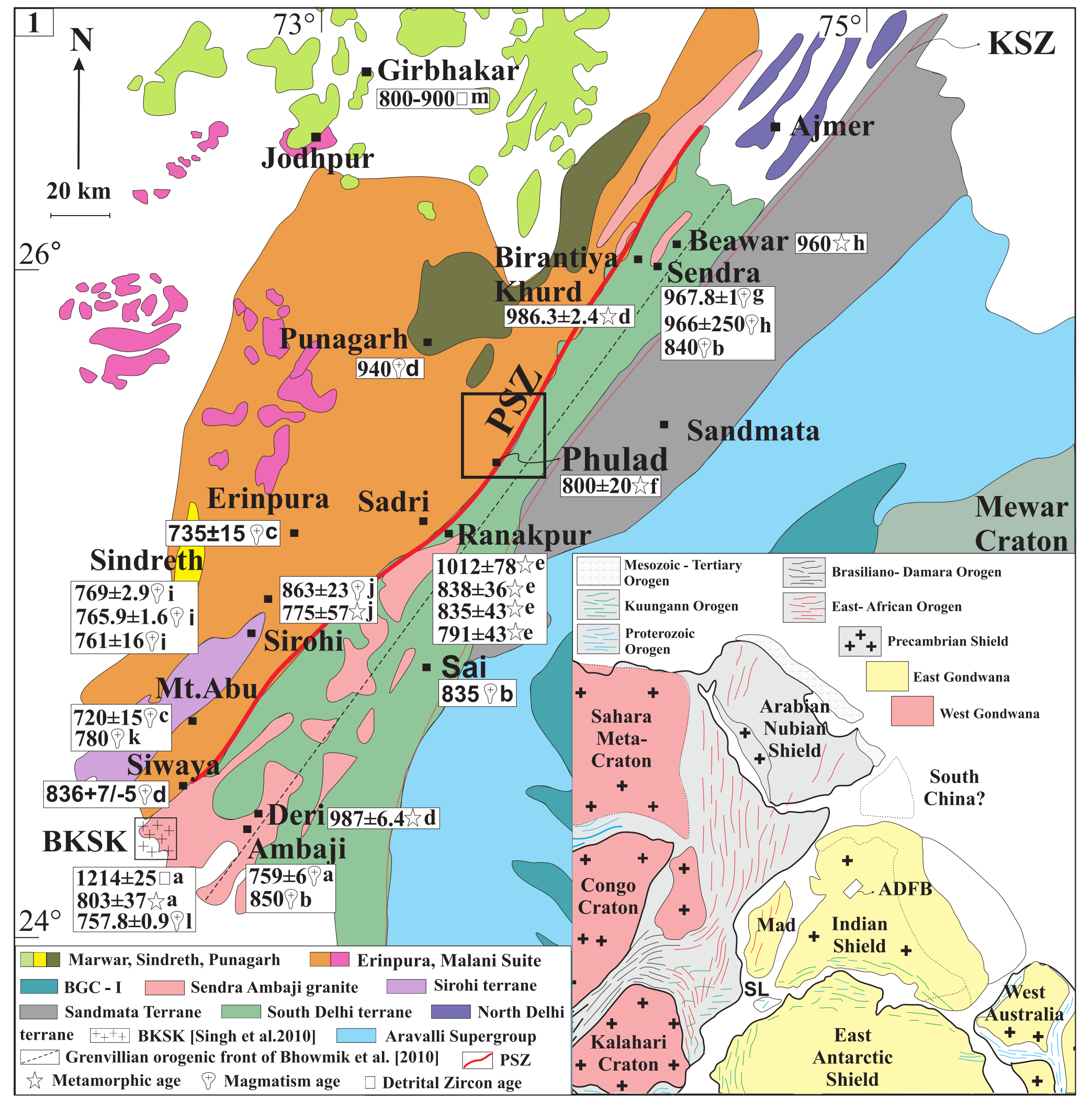

Figure 1. Geological map depicting the different crustal domains in the southern part of the Aravalli Delhi Fold Belt (ADFB) modified after Heron [1953], Gupta et al. [1980], and Roy and Jakhar [2002]. Location of the study area is shown in box. Neoproterozoic magmatic and metamorphic ages (with 2σ errors) in the SDFB and the Marwar Craton are shown in boxes (data source (a) Singh et al. [2010], (b) Choudhary et al. [1984], (c) Crawford [1975], (d) Deb et al. [2001], (e) Volpe and Macdougall [1990], (f) Gangopadhyay and Lahiri [1984], (g) Pandit et al. [2003], (h) Tobisch et al. [1994], (i) Van Lente et al. [2009], (j) Just et al. [2011], (k) Sivaraman and Raval [1995], (l) Roy et al. [2005], and (m) Malone et al. [2008]). Inset showing a part of the dominant orogenic trends and cratons in the Gondwanaland [after Gray et al., 2008, Meert and Lieberman, 2008]. The location of the ADFB in NW India is shown. BKSK: Balaram-Kui-Surpagla-Kengora, PSZ: Phulad Shear Zone, KSZ: Kaliguman Shear Zone.

2. Structures in the Phulad Shear Zone

The PSZ is defined by a narrow zone (25–30 m wide) of intense deformation that juxtaposes the SDFB in the east against the Marwar Craton to the west (Figure 2a, b).

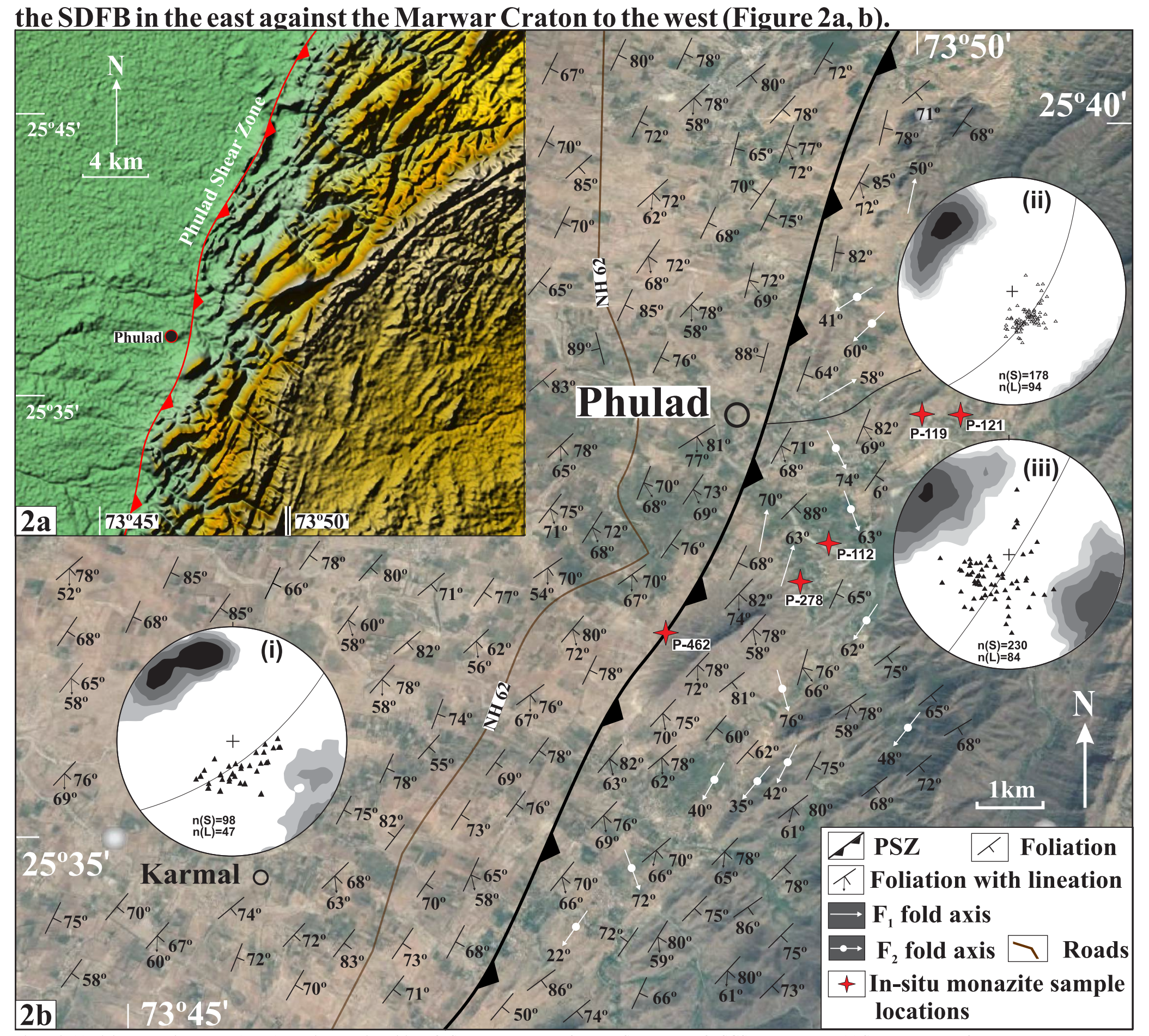

Figure 2. (a) Digital Elevation Model (DEM) showing the disposition of PSZ. DEM prepared from the SRTM data of USGS earth explorer. (b) Structural map of the study area prepared on satellite image of Google Earth. Stereograms showing analysis of structural fabrics collected from entire area (i) Footwall granodiorites, (ii) Phulad Shear Zone, and (iii) Hanging wall rocks. (i) Footwall granodioritic foliations; contour intervals are as follows: 2%, 4%, 8%, and 16% (in increasing shades of gray; max 32.95%). Mean principal orientation is 53°/75°E. (ii) Mylonitic shear zone foliations; contour intervals are as follows: 1%, 2%, 4%, 8%, and 16% (in increasing shades of gray; max 32%). Mean principal orientation is 34°/70°E. (iii) Regional schistosity of the hanging wall rocks; contour intervals are as follows: 1%, 2%, 4%, 8%, and 16% (in increasing shades of gray; max 17.7%). Mean principal orientation is 32°/86°E. Filled triangles are the downdip stretching lineations; n(S) = no. of foliations; n(L) = no. of lineations for all three stereograms.

2.1. Shear Zone Deformation: The PSZ is characterized by extensive development of mylonites in intercalated calcareous and quartzofeldspathic layers (Figure 2c). The mylonitic foliation dips steeply (dip >75°) toward southeast with a prominent set of steep oblique stretching lineations (Figure 2d). Sheath folds with apical directions parallel to the stretching lineation are common (Figure 2e). In the XZ section (subvertical section perpendicular to foliation and parallel to lineation), mesoscopic structures (asymmetric folds) and inclusion trails in pophyroblasts suggest top-to-the-west reverse sense of movement (Figures 2f and 2g). Syntectonic pegmatite veins along the shear zone show pinch and swell structure in both XZ and YZ sections (subhorizontal section perpendicular to foliation and lineation) of the strain ellipsoid (Figure 2h). The aspect ratio of feldspar porphyroclasts in the quartzofeldspathic mylonites in XZ and YZ sections suggests a flattening type of deformation (Figure 2i).

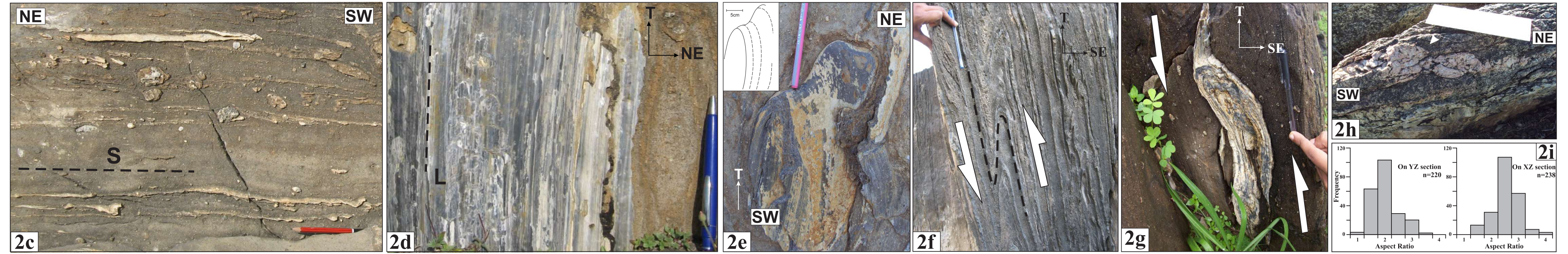

Figure 2. Field photographs of PSZ mylonites. (c) Mylonite foliation in the intercalated calcareous and quartzofeldspathic rock. (d) Downdip lineation in the shear zone foliation. (e) Sheath fold within the PSZ. Pen is aligned parallel to the stretching lineation. Inset shows the line drawing of the sheath fold. (f) Asymmetric folds and (g) asymmetric tail of long tectonic clast showing top-to-the-west reverse sense of movement. (h) Syntectonic pegmatite veins along the shear zone show pinch and swell structure (marked by arrowhead). (i) Histograms showing the aspect ratio of feldspar porphyroclasts in the quartzofeldspathic mylonites in the XZ and YZ sections. The length of the pen/pencil of Figures 3a–3e is 14 cm. n = number of data.

2.2. Footwall Deformation: The lithological-structural, metamorphic, and chronological informations in the Marwar Craton in the PSZ footwall are poorly known. The enclave suite within the granodiorite has WNW trending foliation, oblique to the NE trending PSZ. Rocks of the Marwar Craton in the immediate vicinity of the PSZ are variably deformed granodiorites. The intensity of deformation increases from weakly foliated through gneissose to mylonite and ultramylonite neighboring the PSZ (Figures 2j and 2k). The stretched quartz imparts a strong steep oblique lineation to the rocks (Figure 2l).

Figure 2. Field photographs showing (j) coarse-grained footwall granodiorites distant from the Phulad shear zone. (k) Foliation and (l) downdip stretching lineation of the footwall granodiorites close to the PSZ. The length of the pencil in the photograph 2j and pen in the photograph is 10 cm.

2.3. Hanging Wall Deformation: Distant (~1.5 km) from the PSZ, the hanging wall rocks show two generations of folds (F_1 and F_2). F_1 folds are preserved as rootless hinges (Figure 2m) interfolial to the penetrative schistosity, S_1. This S_1 schistosity is folded giving rise to NE-SW trending F_2 folds with traces of axial plane coplanar with PSZ mylonitic foliation. The fold axes of F_2 folds vary considerably from subhorizontal to subvertical (Figures 2n, 2o and 2q). At places the curved nature of the F_2 fold hinges forming sheath folds is obvious (Figure 2p). The formations of the large-scale F_2 sheath folds are likely to have occurred during the top-to-the-west reverse sense of movement (Figure 2r). Close to the PSZ, the rocks show strong development of a single foliation and a steep oblique lineation parallel to the mylonitic fabrics in the PSZ (Figure 2s).

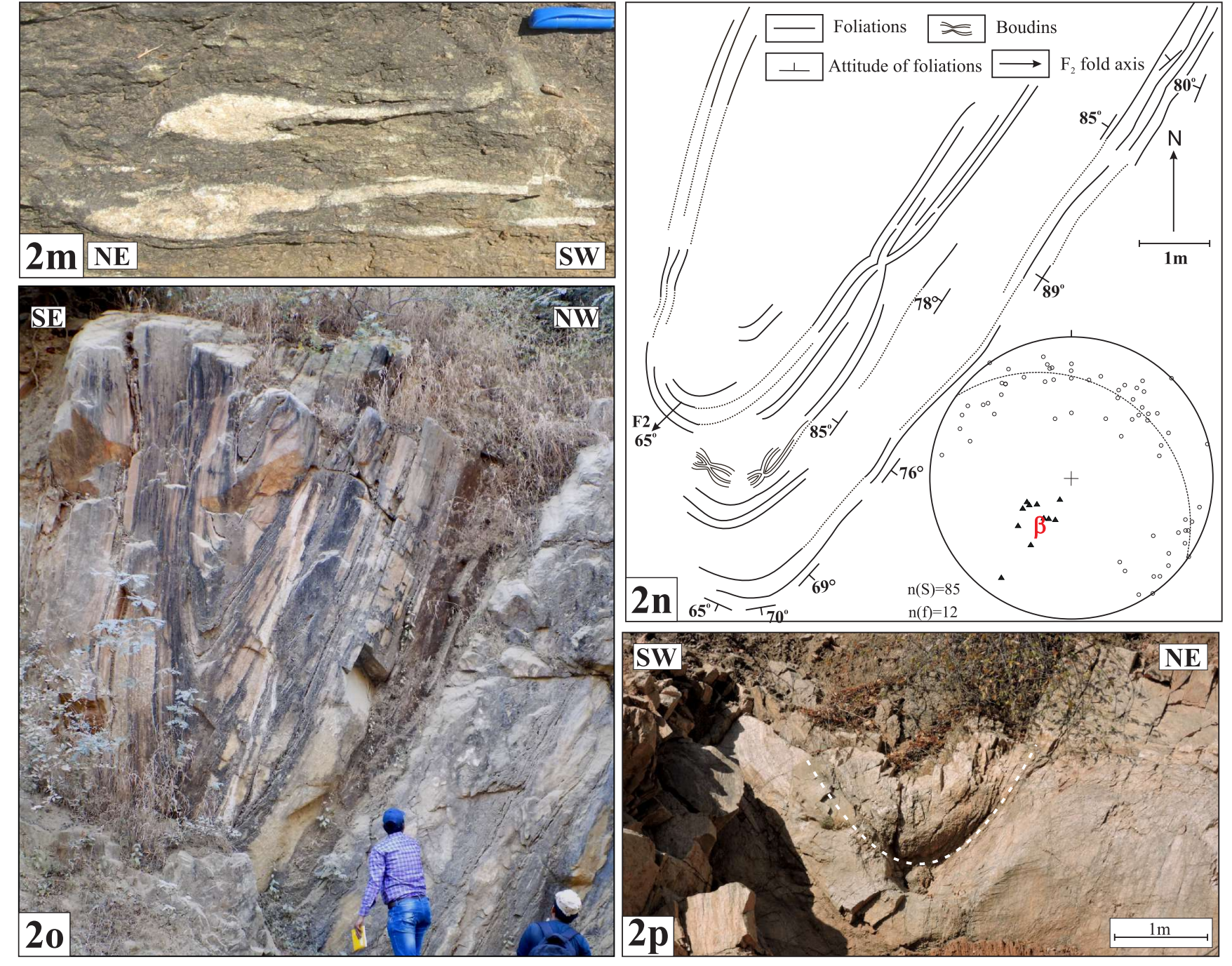

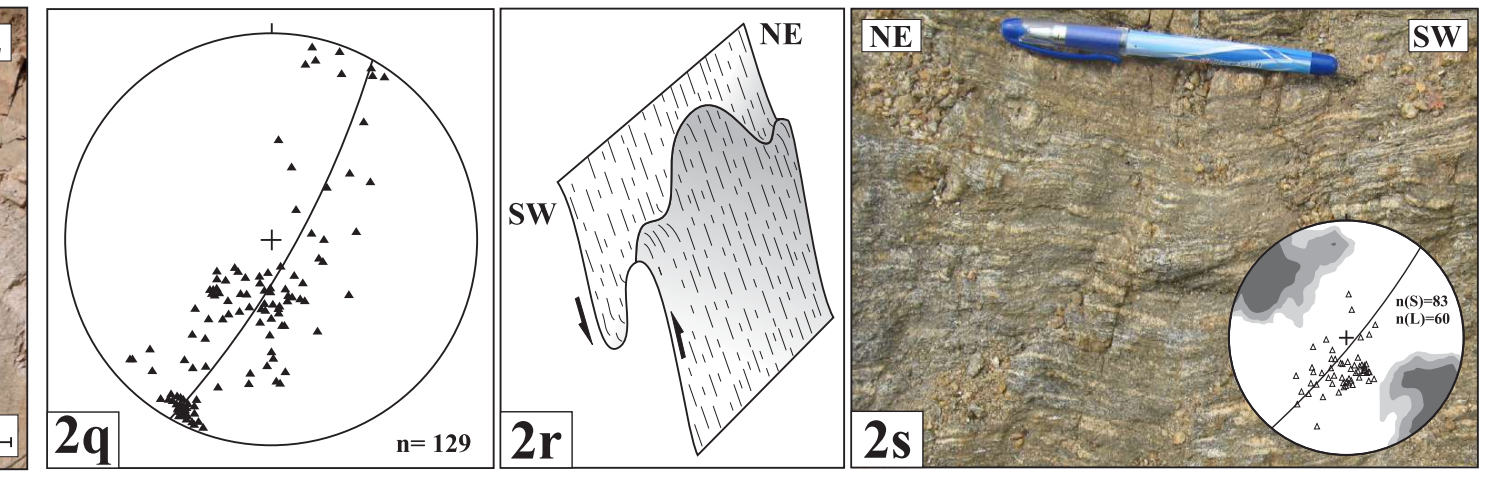

Figure 2. Field photographs showing (m) rootless F_1 fold in metamarl. (n) Outcrop scale map of F_2 isoclinal folds. Note the presence of boudins at the hinge of the fold. Stereogram showing regional F_2 folds with F_2 folds axes (filled triangles). The calculated β axis corresponding to the girdle is 057°→216°W. (o) Profile section of a large-scale upright F_2 fold. (p) Field photograph showing a large scale sheath fold with sharp curvature of the hinge of sheath fold (marked as white dash line). (q) Stereogram showing the plot for the F_2 fold axes (closed triangles). (r) Schematic diagram showing the development of sheath fold with top-to-the-west reverse sense of movement. (s) Field photographs showing mica schists with closely spaced schistosity that is parallel to the mylonitic foliation in the shear zone, stereogram showing the regional schistosity of the hanging wall rocks; contour intervals are as follows: 2%, 4%, and 8% (in increasing shades of gray; max 16.87%). Mean principal orientation [illegible] cap/pen in Figure [illegible] n(S) = number of foliations data; n(L) = number of fold axes data.

3. Petrography and Mineral Chemistry

The mica schists in and neighboring the PSZ are characterized by foliation parallel alternate bands of mica-rich layers (M-domain) and quartz-rich layers (Q-domain). At PSZ, the rock shows single fabric ($S_1 \| S_2$) (Figure 3a). However, distant from the shear zone (~1.5 km), two sets of planar fabrics S_1 and S_2 are identified. The S_1 schistosity is preserved as the interfolial domain of the S_2 schistosity (Figure 3b) and as internal trails within pre-S_2 garnet porphyroblasts (Figure 3c). Garnet porphyroblasts occur both in Q-domain and M-domain. In Q-domain the garnet porphyroblasts are large and inclusion rich. Figure 3c shows the straight internal schistosity (Si) makes a high angle to the external schistosity (Se). The external S_2 schistosity wraps around the garnet porphyroblast, indicating that growth of garnets is pre-kinematic with respect to S_2. However, the margins of the pre-S_2 garnets with well-developed dodecahedral faces overgrow the warped S_2 schistosity. M-domain garnets are comparatively small and sub-idioblastic to idioblastic in shape. The porphyroblasts with no included minerals overgrew the S_2 schistosity in M-domain suggesting that they grew post-S_2 (Figure 3d). Garnet porphyroblasts with dodecahedral faces overgrowing the S_2 schistosity often show straight inclusion trail pattern that are continuous with S_2 external schistosity (Figure 3e). This implies that the growth of garnet is syn to post-kinematic with respect to S_2.

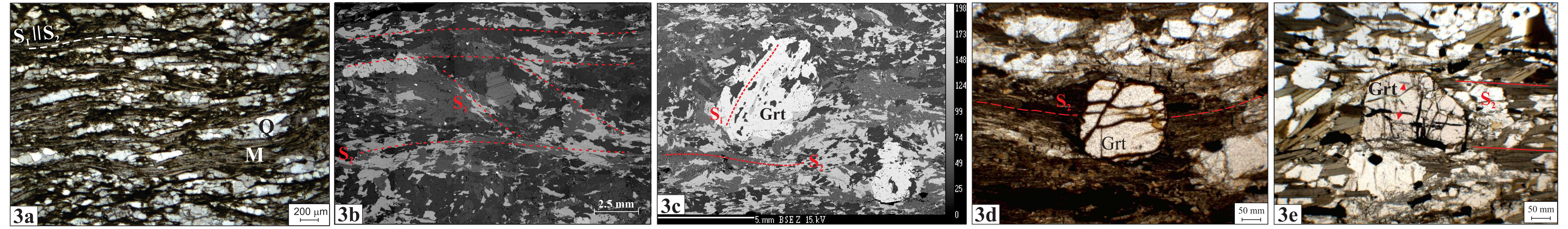

Figure 3. Photomicrograph in (a, d, and e) PPL, in (b and c) BSE. (a) Mica schists with well-developed alternate bands of muscovite-rich (marks as M) and quartz-rich (marks as Q) domain. (b) BSE image of mica schist showing relict S_1 schistosity in S_2 interfolial domain. (c) Q-domain garnet porphyroblasts with inclusion trails at high angle to the warping S_2 schistosity. (d) M-domain garnet with no included minerals overgrew the external S_2 schistosity. (e) Straight inclusion trails within the M-domain garnet that is continuous with the external S_2 schistosity. Sillimanite grains included within garnet porphyroblasts are marked by red arrow head. PPL: Plane Polarized light image, BSE: Back scatter electron.

The mica schists show diverse mineralogical assemblages and are divided into three groups based on the presence or absence of particular mineral assemblages. These are as follows:

A. garnet–biotite–muscovite–plagioclase–quartz–K-feldspar–ilmenite
B. garnet–sillimanite–biotite–muscovite–plagioclase–quartz–K-feldspar–ilmenite
C. garnet–kyanite–sillimanite–biotite–plagioclase–quartz–muscovite–K-feldspar–ilmenite–magnetite

Porphyroblasts of garnet (pre-S_2 to post-S_2) contain quartz, biotite and ilmenite as included minerals (Figure 3c) in assemblage A. In assemblage B and C, garnet porphyroblasts (pre-S_2 to post-S_2) contain quartz, biotite, sillimanite and ilmenite as included minerals (Figure 3e). In assemblage C, kyanite grains occur as porphyroblasts mainly in the M-domain. Kyanite directly abuts the S_2 schistosity forming a helicitic texture (Figures 3f and 3g). Porphyroblasts of muscovite with few biotites often occur at the hinge of F_2 folds without any evidence of deformation (Figure 3h). Textural relations indicate that kyanite along with few muscovites and biotite porphyroblasts grew post with respect to the fabric (S_1 and S_2) forming event.

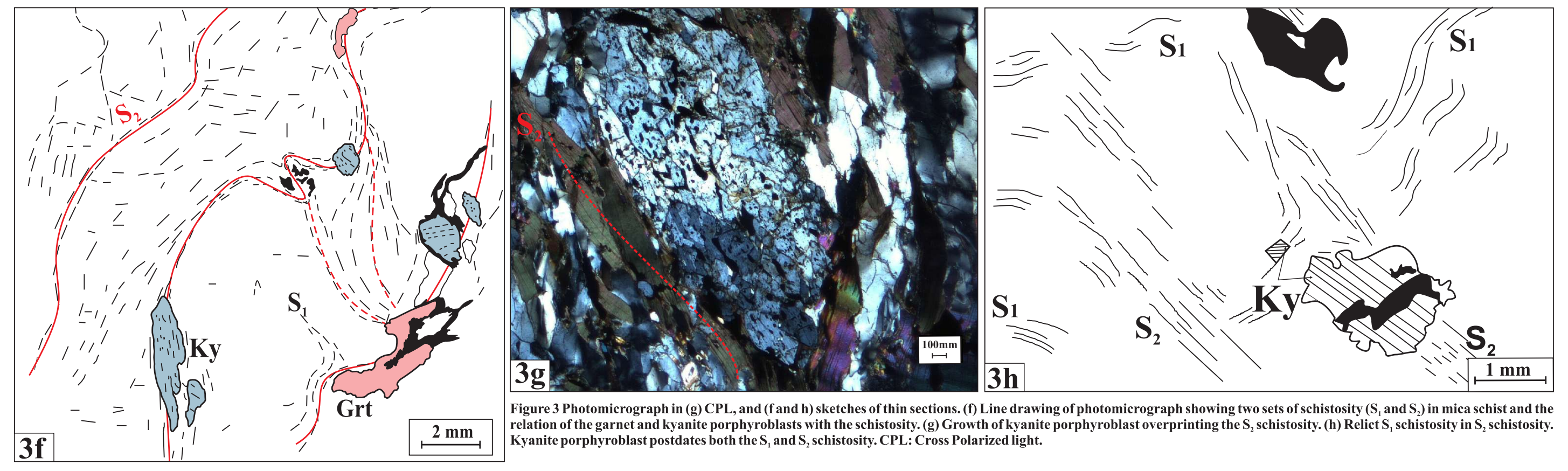

Figure 3 Photomicrograph in (g) CPL, and (f and h) sketches of thin sections. (f) Line drawing of photomicrograph showing two sets of schistosity (S_1 and S_2) in mica schist and the relation of the garnet and kyanite porphyroblasts with the schistosity. (g) Growth of kyanite porphyroblast overprinting the S_2 schistosity. (h) Relict S_1 schistosity in S_2 schistosity. Kyanite porphyroblast postdates both the S_1 and S_2 schistosity. CPL: Cross Polarized light.

Garnet in the mica schists are almandine rich, X_{Fe} (= Fe/ΣX$_i$, where i= Fe+Mg+Mn+Ca) varying between 0.80 and 0.85. Garnet exhibits rimward decrease of X_{Ca} and X_{Mg}, whereas X_{Fe} and X_{Mn} show the opposite trend (Figure 3i-3n; assemblages A). The variations are small and gradual in the interiors in the Q-domain porphyroblasts, but the variations in the margins of these porphyroblasts overgrowing the S_2 shear zone fabric are more pronounced. The compositions of the rims are similar to the smaller post-S_2 M-domain porphyroblasts (Figure 3i, k).

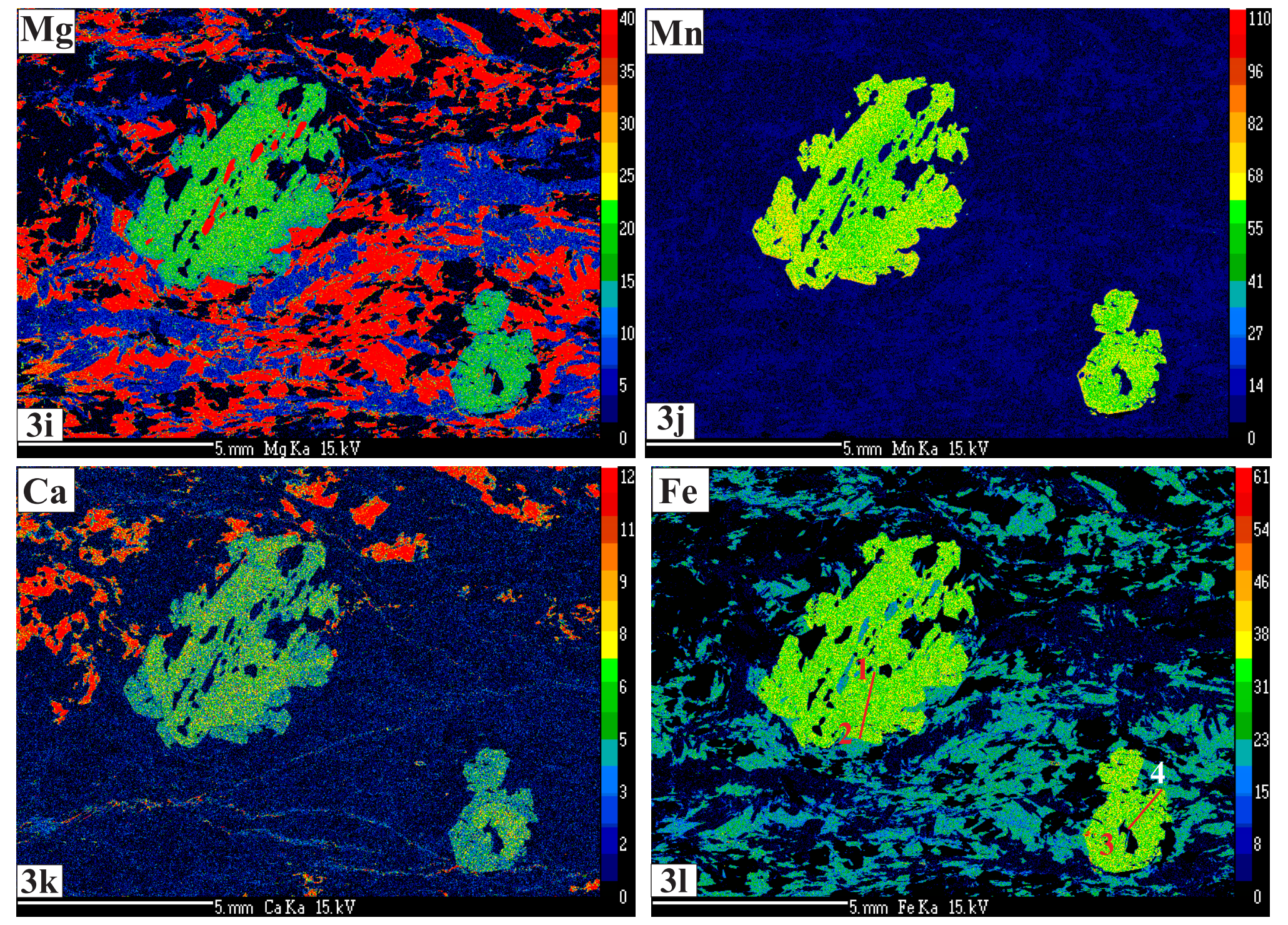

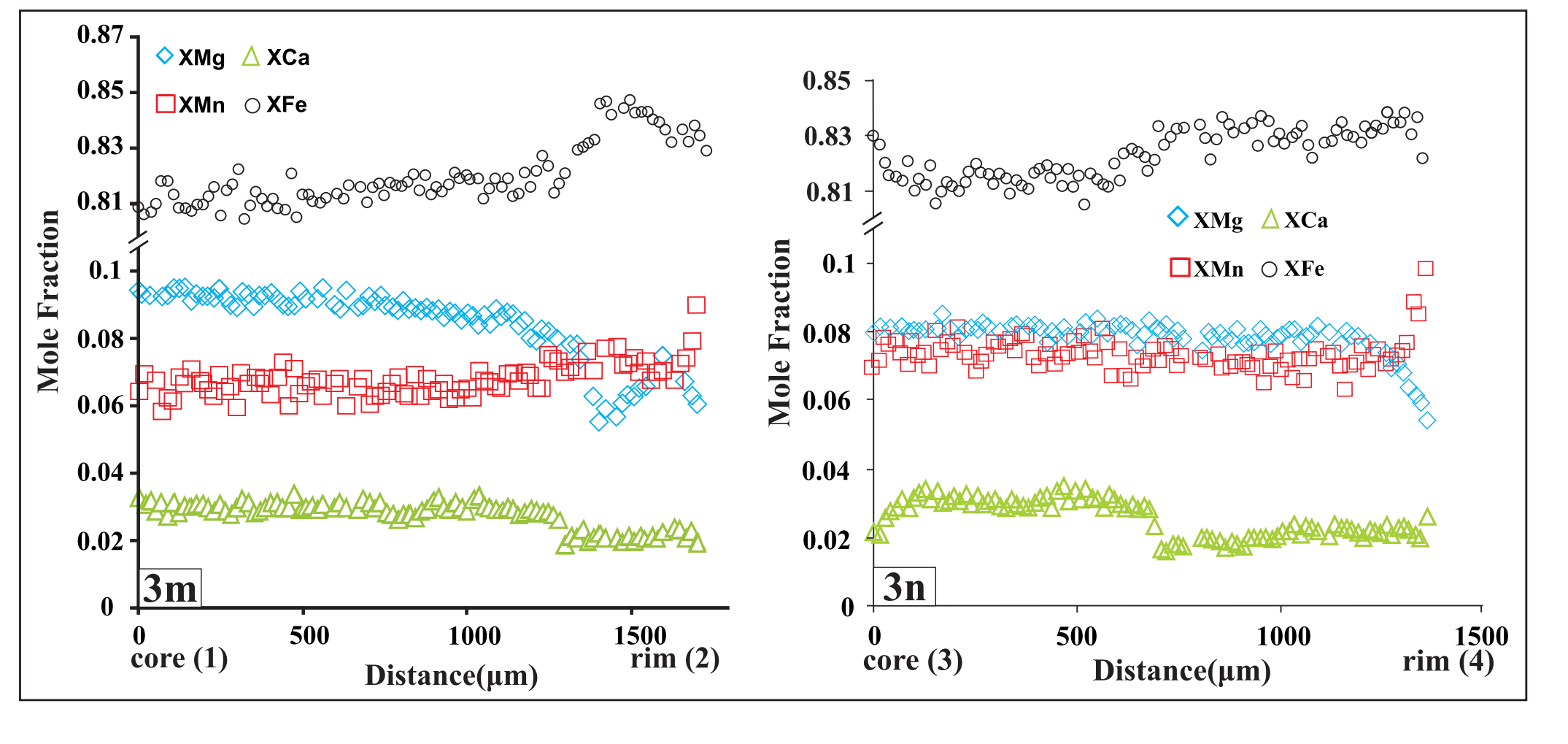

Figure 3. (i–l) Mg, Mn, Ca, and Fe X-ray element maps of the garnet porphyroblast from the assemblage A (sample no. P-278). (m–n) Core to rim variations in mole fractions of pyrope, spessartine, grossular, and almandine along the red line (1 – 2 and 3–4 of Figure 3l), respectively.

4. P-T Estimation

Temperatures were estimated using the garnet-biotite thermometer [Bhattacharya et al., 1992, GS] and the muscovite-biotite geothermometer based on Mg-Tschermak's substitution [Hoisch, 1989]. The core and rim temperatures for pre-S_2 garnet-biotite pair were 640 ± 10°C and 600 ± 10°C, respectively and the corresponding temperatures for post-S_2 garnet-biotite pair were 630 ± 10°C and 580 ± 12°C, respectively. Temperatures (570 ± 50°C; P-278, assemblage A) estimated for the schists using the Mus-Bt thermometry are somewhat lower than those estimated using the biotite-garnet thermometers. In view of the low grossular contents in garnet (< 5 mol %) and the Na-rich nature of plagioclase (An <16 mol %), the barometers could not be applied to estimate metamorphic pressure.

P-T pseudosection in MnNCKFMASH system was constructed for bulk rock composition of the sillimanite-free assemblage A (P-278) mica schists using mole proportion of oxides of whole rock by modal analysis. The PERPLEX program of Connolly [2005] (updated in 2009) was used for computation of the pseudosection using the internally consistent database of Holland and Powell [1998]. The fluid phase was taken to be pure H_2O and occurs in excess. Figure 4 shows the stability field of different mineral assemblages in the given P-T window. The topology of the stable phase fields and the theoretically determined isopleths for mole fractions of garnets in the P-T pseudosections are combined with measured compositions of zoned garnets (Figure 3i-l) to retrieve the P-T paths experienced by the rocks (Figure 4). The retrieved P-T paths show near-isothermal (T ~ 670°C) decompression at midcrustal depths (6–8 kbar) for compositions of Q-domain garnet interiors, followed by cooling consistent with the compositions of M-domain post-S_2 garnets and mantles around Q-domain pre-S_2 garnets (Figure 3i-l). The cooling episode is consistent with the occurrence of post-S_2 kyanite porphyroblasts, in assemblage C. In the absence of anatexis and metamorphic K-feldspar in the mica schists, the decompression and cooling history is likely to have taken place in the retrograde portion of a clockwise P-T path (Figure 4) involving loading-heating as a consequence of top-to-the west reverse movement in the PSZ.

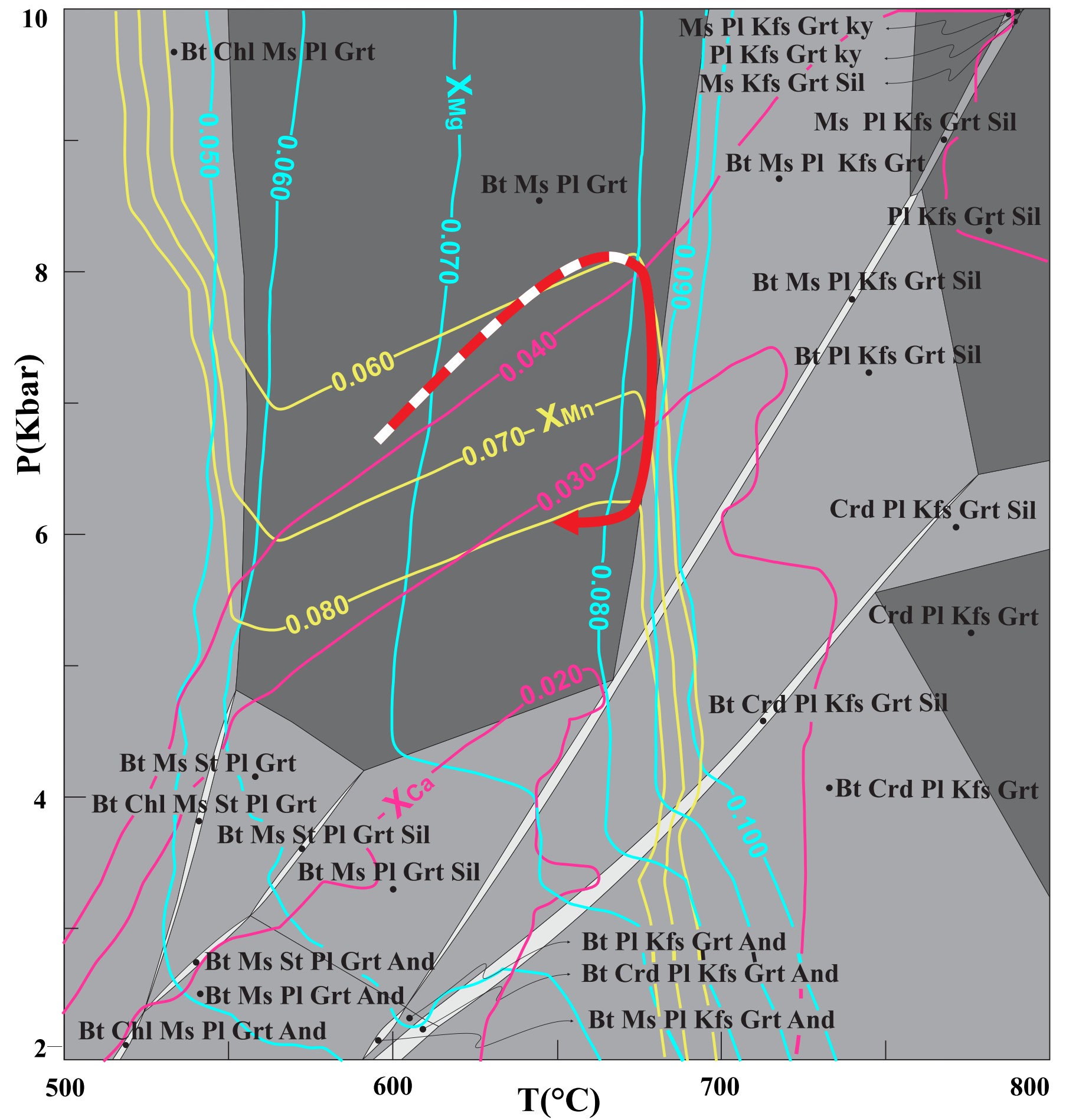

Figure 4. P-T pseudosection in MnNCKFMASH system showing the stability fields of the mineral assemblages for the bulk rock composition Na_2O = 1.43, CaO = 0.55, K_2O = 5.18, FeO = 11.35, MgO = 1.99, and Al_2O_3 = 17.92, SiO_4 = 58.88 (values mole proportions of system components recalculated to 100) of assemblage A (Sample No: P-278). The darkest shade corresponds to low variance fields; progressively lighter shades are for higher variance fields. X_{Ca}, X_{Mg}, and X_{Mn} isoplets of garnet composition in the P-T pseudosection in MnNCKFMASH system. The bold red arrow indicates the possible path.

5. Monazite Age Determinations

In the mica schists, monazites occur both within garnet porphyroblasts and in the matrix (Figure 5). Trails of prismatic monazite parallel to inclusion trails of other minerals are common within both Q- and M-domain garnets (Figures 5a and 5b). In the matrix, lineated monazites with margins discordant to the warping foliation are also common (Figures 5f–5i). Monazites in the pegmatite are 50 to 150 µm in diameter. The monazite exhibits strongly resorbed margins; i.e., xenotime and huttonite/thorite embedded in apatite form coronae around monazite grains (Figures 5j and 5k) and xenotime-huttonite/thorite aggregates also occur as veins within the monazite grains.

In the mica schists, the probability density plot for all spot ages (number of spots, 125) taken together is shown in Figure 5l. The ages in the four samples can be statistically resolved into two distinct populations, e.g., 970 ± 9 Ma (MSWD = 0.92) and 809 ± 7 Ma (MSWD = 1.6). There is no difference in age populations between monazites hosted within the porphyroblasts and in the mineralogically differentiated matrix. By contrast, all monazite spot ages (number of spots, 37) in the syntectonic pegmatite correspond to a single age group, e.g., 810 ± 6 Ma (n = 37, MSWD = 0.53; Figure 5m).

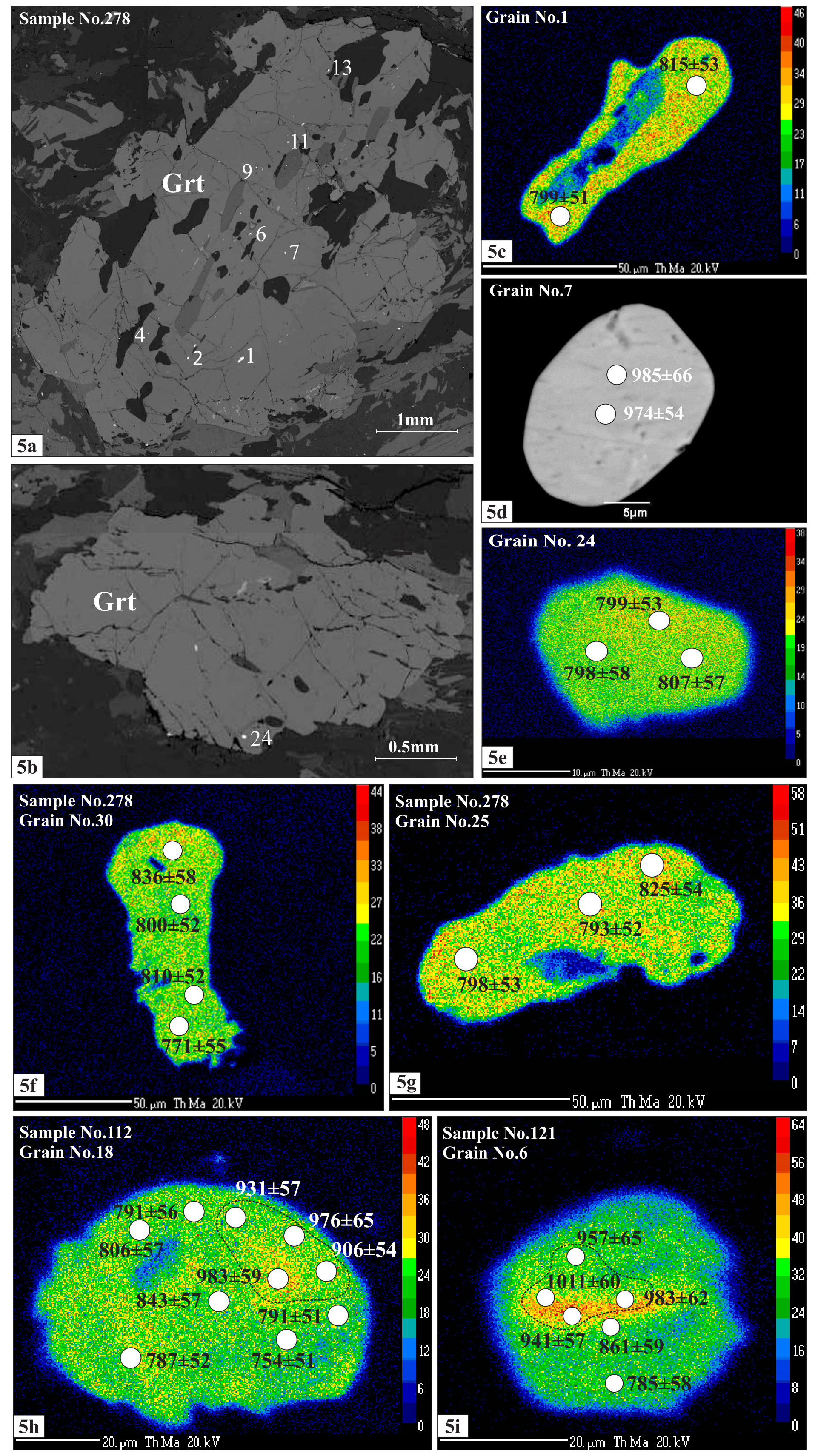

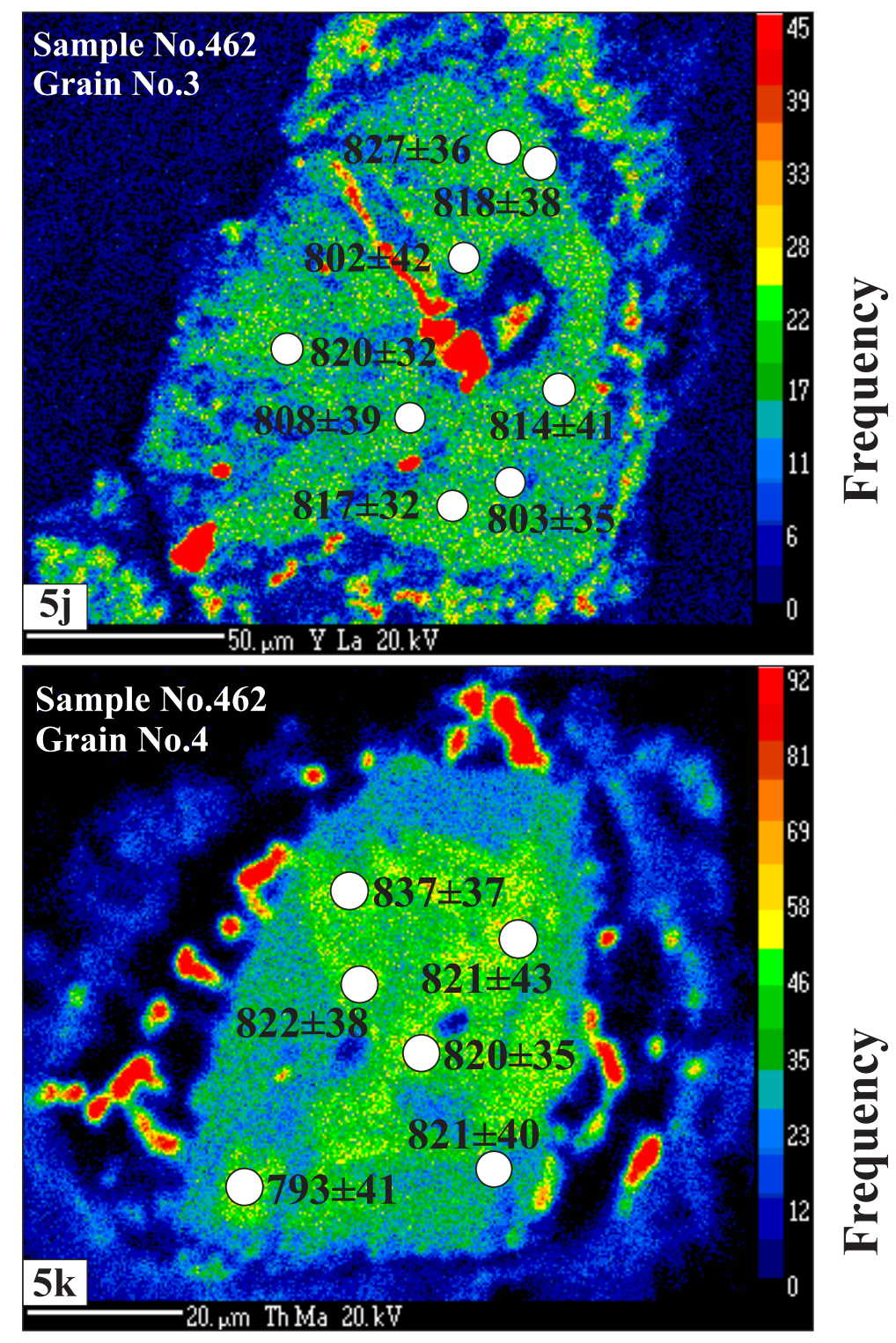

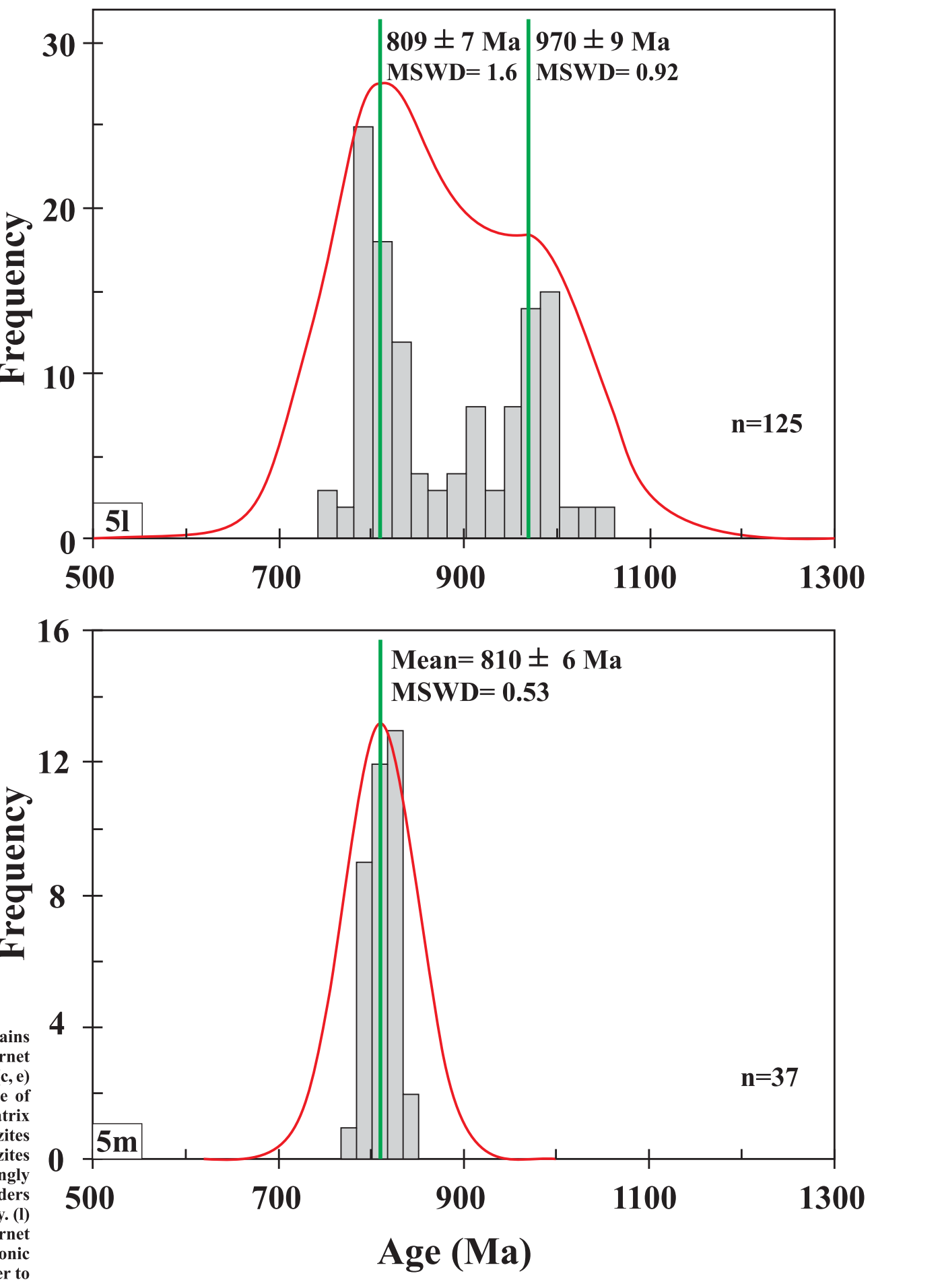

Figure 5. BSE images of (a) the pre-S_2 garnet porphyroblast shows monazite grains aggregates which are parallel to the inclusion trails of other minerals within the garnet and (b) the post-S_2 garnet porphyroblast showing the position of the monazite grain. (c, e) Th X-ray maps of representative monazites hosted within garnet. (d) BSE image of representative monazite grain hosted within garnet. (f–i) Th X-ray maps of matrix monazites in the mica schists. Note that older age domains within these matrix monazites are marked with broken lines. (j) Y and (k) Th X-ray maps of representative monazites within the syntectonic pegmatites. Note that the monazite grains exhibit strongly resorbed margins with xenotime vein in Figure 5j. White filled circles with black borders and keyed numbers are locations of analyzed spots and spot ages in Ma, respectively. (l) Plot of relative probability and frequency of spot ages in monazites sequestered in garnet as well as in the matrix within mica [schists and (m) monazites within syntectonic pegmatites, obtained using Isoplot/Ex [Ludwig, 2003]. Numbers keyed to peaks refer to statistically unmixed peak ages (±2σ error) in Ma of spot age population in the three types of monazites. n = number of spot age determinations.

6. Discussion

In calcareous and quartzofeldspathic mylonites in and around Phulad, the shear zone is characterized by steep SE dipping mylonitic fabric and a steep oblique stretching lineation. The shear zone is developed in a ductile regime with top-to-the-west reverse sense of movement coupled with pronounced flattening across the PSZ.

MnNCKFMASH pressure-temperature pseudosection analysis of closely spaced specimens of garnet-bearing mica schists reveals that the stabilization of syn/post-garnet porphyroblasts in the hanging wall experienced near-isothermal decompression followed by cooling in the retrograde arm of a clockwise P-T path. The retrieved P-T paths are consistent with reverse motion of SDFB mica schist over the cratonic foreland. U-Th-Pb (total) monazite age determinations in hanging wall mica schists indicate that reverse motion on the PSZ occurred at 810 ± 6 Ma. The pre-shearing Grenvillian age (~970 ± 9 Ma) metamorphic monazites of the SDFB occur as embayed cores, in the interiors of younger monazite grains. Intense high-temperature deformation and the emplacement of mica-bearing pegmatites during reverse shearing caused recrystallization of monazites by dissolution-precipitation, mantling older monazites in the hanging wall SDFB schists.

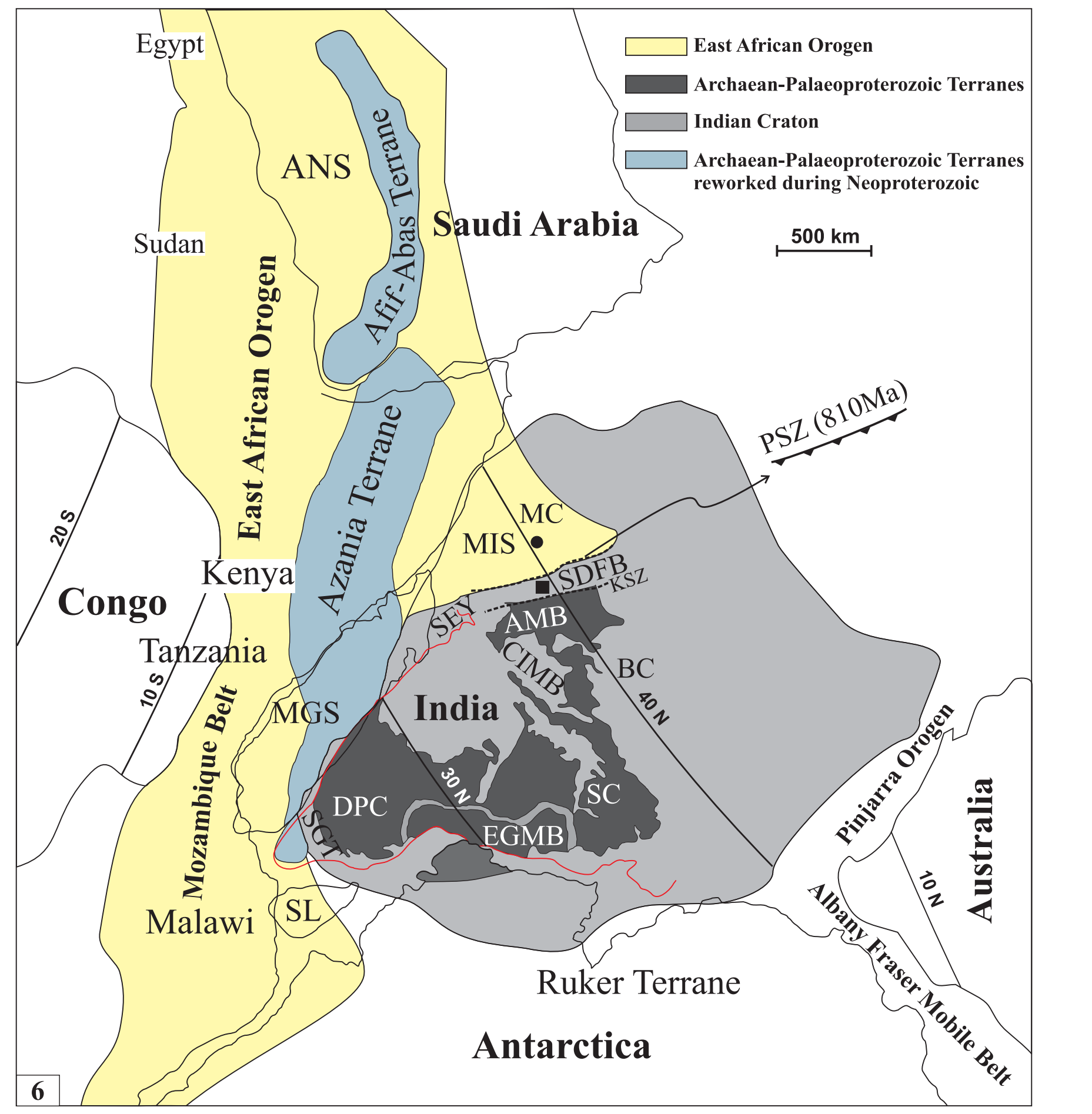

Figure 6. Geological map showing the East African Orogen and various cratonic blocks after Fitzsimons [2003a, 2003b], Johnson and Woldehaimanot [2003], Collins and Pisarevsky [2005], and Singh et al. [2010]. The palaeolatitude lines are superimposed from Meert [2003]. ANS: Arabian-Nubian shield, AMB: Aravalli Mobile Belt, BC: Bundelkhand Craton, CIMB: Central India Mobile Belt, DPC: Dharwar Protocontinent, EGMB: Eastern Ghats Mobile Belt, KSZ: Kaliguman Shear Zone, MGS: Madagascar, MC: Marwar Craton, PSZ: Phulad Shear Zone, SC: Singhbhum Craton, SEY: Seychelles, SGT: Southern Granulite Terrane, SL: Sri Lanka.

6.1. Regional Implications

Palaeomagnetic studies from Malani Igneous Suite (MIS) in the Marwar Craton (~771 Ma) [Torsvik et al., 2001a] and magmatic rocks in Seychelles (~750 Ma) [Tucker et al., 2001] suggest close palaeopole positions of NW India and Seychelles [Torsvik et al., 2001a, 2001b] during mid-Neoproterozoic (Figure 6). Tucker et al. [1999] suggest that Seychelles-MIS composite and northern parts of Madagascar may comprise a separate terrane during the mid-Neoproterozoic, ~750 Ma. If MIS-Seychelles-North Madagascar was a coherent terrane separate from the remaining parts of the present-day Peninsular India at ~750 Ma, then the palaeopole position of MIS older than 750 Ma would not be applicable for the Greater India landmass. Therefore, it appears that a suture is likely to exist along which the Marwar Craton amalgamated with the remaining India. However, the timing and suturing of the MIS hosting Marwar Craton with the remaining India remains speculative. Studies from the ADFB in northwestern India provide evidence of a Grenvillian age collisional orogen between Marwar Craton to the west and North Indian Block to the east [Bhowmik et al., 2010]. However, the new data presented in this study indicate that the SDFB preserves the Grenvillian age history with the mid-Neoproterozoic history restricted to the western margin of SDBF along PSZ. It is suggested that the PSZ appears to be the most likely locale along which the Greater India landmass accreted with the Marwar Craton at ~810 Ma. Therefore, it appears that the ~770 Ma palaeopole position obtained in MIS represents the location of Greater India postdating the accretion along PSZ at ~810 Ma.

Acknowledgment: SMC acknowledges the Department of Science and Technology, New Delhi (India), for financial support

References:

Bhattacharya, A., L. Mohanty, A. Maji, S.K. Sen, and M. Raith (1992), Non-ideal mixing in the phlogopite-annite binary: constraints from experimental data on Mg-Fe partitioning and a reformulation of the biotite-garnet geothermometer. Contribution to Min. and Petro., 111, 87–93.
Bhowmik, S.K., H.J. Bernhardt, and S. Dasgupta (2010), Grenvillian age high-pressure upper amphibolite-granulite metamorphism in the Aravalli-Delhi Mobile Belt, Northwestern India: New evidence from monazite chemical age and its implication. Precambrian Res., 178, 168–184.
Choudhary, A.K., K. Gopalan, and C.A. Sastry (1984), Present status of the geochronology of the Precambrian rocks of Rajasthan. Tectonophysics, 105, 131–140.
Collins, A.S., and S.A. Pisarevsky (2005), Amalgamating eastern Gondwana: the evolution of the Circum Indian Orogens. Earth Sci. Rev., 7, 229–270.
Connolly, J.A.D. (2005), Computation of phase equilibria by linear programming: a tool for geodynamic modeling and its application to subduction zone decarbonation. Earth Planet. Sci. Lett., 236, 524-541.
Crawford, A.R. (1975), Rb–Sr age determination for the MountAbu Granite and related rocks of Gujarat. J. Geol. Soc. India 16, 20–28.
Deb, M., R.I. Thorpe, D. Kristic, F. Corfu, D.W. Davis, (2001), Zircon U-Pb and galena Pb isotope evidence for an approximate 1.0 Ga terrane constituting the western margin of the Aravalli-Delhi orogenic belt, northwestern India. Precambrian Res., 108, 195–213.
Fitzsimons, I.C.W. (2003a), Does the late Neoproterozoic Darling Fault Zone of Western Australia extend all the way to the Transantarctic Mountains? SGTSG Field meeting. Abstracts- Geological Society of Australia 72, 130 (Kalbarri).
Fitzsimons, I.C.W. (2003b). Proterozoic basement provinces of southern and southwestern Australia, and their correlation with Antarctica. In: Yoshida, M., Windley, B.F., Dasgupta, S. (Eds.), Proterozoic East Gondwana: Supercontinent Assembly and Breakup. Special Publication Geol. Soc. of London, pp. 93–130.
Gangopadhyay, P.K., and A. Lahiri (1984), Earth's crust and evolution of the Delhi Supergroup in central Rajasthan. In: Proceedings of the seminar on Crustal evolution of Indian shield and its bearing on metallogeny. Indian J. of Earth Sci., 92–113.
Ganguly, J., and S.K. Saxena (1984), Mixing properties of aluminosilicategamets: constraints from natural and cxperimental data, applications to geothermo-barometry. American Mineralogist 69, 88-97.
Gray, D.R., D.A. Foster, J.G. Meert, B.D. Goscombe, R. Armstrong, R.A.J. Truow, and C.W. Passchier (2008), A Damaran perspective on the assembly of southwestern Gondwana. Geol. Soc. London Special Publications, 294, 257-278. Gujarat. J. Geol. Soc. India 16, 20–28.
Gupta, S.N., Y.K. Arora, R.K. Mathur, P.B. Iqballuddin, T.N. Sahai, and S.B. Sharma (1980), Lithostratigraphic map of Aravalli region. Geol. Survey of India, Calcutta. Scale 1:1,000,000.
Heron, A.M. (1953), Geology of Central Rajputana. Memoir Geological Survey India 79, 339.
Hoisch, T.D. (1989), A muscovite-biotite geothermometer. American Mineralogist 74, 565-572.
Holland, T.J.B., R. Powell, (1998), An internally consistent thermodynamic data set for phases of petrological interest. J. of Metamorphic Geol.,16, 309–343.
Johnson, P.R., and B. Woldehaimanot (2003), Development of the Arabian-Nubian Shield: perspectives on accretion and deformation in the northern East African Orogen and the assembly of Gondwana. In: Yoshida, M., Windley, B.F., Dasgupta, S. (Eds.), Proterozoic East Gondwana: Supercontinent Assembly and Breakup, 206. Geol. Soc. London Special Publication, 289–325.
Just, J., B. Schulz, H. de Wall, F. Jourdan, and M. K. Pandit (2011), Monazite CHIME/EPMA dating of Erinpura granitoid deformation: Implications for Neoproterozoic tectono-thermal evolution of NW India. Gondwana Res., 19, 402–412.
Ludwig, K.R. (2003), Isoplot/EX version 3.0, A geochronological toolkit for Microsoft Excel: Berkeley Geochronology Center Special Publication 1a.
Malone, S.J., J.G. Meert, D.M. Banerjee, M.K. Pandit, E. Tamrat, G.D. Kamenova, V.R. Pradhana, and L.E. Sohl (2008), Paleomagnetism and Detrital Zircon Geochronology of the Upper Vindhyan Sequence, Son Valley and Rajasthan, India: a ca. 1000Ma Closure age for the Purana Basins? Precambrian Res. 164, 137–159.
Meert J.G., and B.S. Lieberman (2008), The Neoproterozoic assembly of Gondwana and its relationship to the Ediacaran–Cambrian radiation. Gondwana Res., 14, 5–21.
Meert, J.G., (2003), A synopsis of events related to the assembly of eastern Gondwana. Tectonophysics 362, 1 – 40.
Pandit, M.K., L.M. Carter, L.D. Ashwal, R.D. Tucker, T.H. Torsvik, B. Jamtveit, and S.K. Bhushan (2003), Age, petrogenesis and significance of 1Ga granitoids and related rocks from the Sendra area, Aravalli Craton, NW India. J. Asian Earth Sci., 22, 363–381.
Roy, A.B., A. Kröner, V. Laul, and R. Purohit (2005), Single zircon dating of hypersthenes bearing granitoid from Balaram-Abu Road area, southern part of the Aravalli Mountains. In: Thomas, H. (Ed.), NW India—Implication for Malani Magmatism related thermal event, in Metamorphism and Crustal Evolution. Atlantic Publishers and Distributors, New Delhi, pp. 339–346.
Roy, A.B., and S.R. Jakhar (2002), Geology of Rajasthan (Northwest India) Precambrian to recent. Scientific Publishers, Jodhpur, India, 205 pp.
Singh, Y.K., B.D. Waele, S. Karmakar, S. Sarkar, T.K. Biswal (2010), Tectonic setting of the Balaram-Kui-Surpagla-Kengoragranulites of the South Delhi Terrane of the Aravalli Mobile Belt, NW India and its implication on correlation with the East African Orogen in the Gondwana assembly. Precambrian Res., 183, 669–688.
Sivaraman, T.V., and U. Raval (1995), U–Pb isotopic study of zircons from a few granitoids of Delhi–Aravalli belt. J. Geol. Soc. India, 46 (5), 461–475.
Tobisch, O.T., K.D. Collerson, T. Bhattacharya, and D. Mukhopadhyay (1994), Structural relationship and Sm–Nd isotope systematics of polymetamorphic granitic gneisses and granitic rocks from central Rajasthan, India—implications for the evolution of the Aravalli craton. Precambrian Res., 65, 319–339.
Torsvik, T.H., L.D. Ashwal, R.D. Tucker, and E.A. Eide (2001a), Neoproterozoic geochronology and palaeogeography of the Seychelles microcontinent: the India link. Precambrian Res., 110, 47–59.
Tucker, R.D., L.D. Ashwal, and T.H. Trosvik (2001), U-Pb geochronology of Seychelles granitoids: a neoproterozoic continental arc fragment. Earth And Planet. Sci., 185, 27-38.
Tucker, R.D., L.D. Ashwal, M.J. Handke, M. Hamilton, M. Le Grange, R.A. Rambeloson (1999), U-Pb geochronology and isotopegeochemistry of the Archean and Proterozoic rocks of northcentral Madagascar. J., Geol., 107, 135–153.
Van L.B., L.D. Ashwal, M.K. Pandit, S.A. Bowring, and T.H. Torsvik (2009), Neoproterozoic hydrothermally altered basaltic rocks from Rajasthan, northwest India: Implications for late Precambrian tectonic evolution of the Aravalli craton; Precambrian Res., 170, 202–222.
Volpe, A.M., and J.D. Macdougall (1990), Geochemistry and isotopic characteristics of mafic (Phulad ophiolite) and related rocks in the Delhi Supergroup, Rajasthan, India: implications for rifting in the Proterozoic. Precambrian Res., 48, 167–191.